

RESEARCH

Open Access



Integrated omics characterization reveals reduced cancer indicators and elevated inflammatory factors after thermal ablation in non-small cell lung cancer patients

Xinglu Zhang^{1†}, Shuai Shao^{1†}, Nan Song², Baolu Yang¹, Fengjiao Liu¹, Zhaohui Tong^{1,2*}, Feng Wang^{1*} and Jieqiong Li^{2*}

Abstract

Background Thermal ablation is a minimally invasive treatment for non-small cell lung cancer (NSCLC). Aside from causing an immediate direct tumour cell injury, the effects of thermal ablation on the internal microenvironment are unknown. This study aimed to investigate the effects of thermal ablation on the plasma internal environment in patients with NSCLC.

Methods 128 plasma samples were collected from 48 NSCLC (pre [LC] and after thermal ablation [LC-T]) patients and 32 healthy controls (HCs). Olink proteomics and metabolomics were utilized to construct an integrated landscape of the cancer-related immune and inflammatory responses after ablation.

Results Compared with HCs, LC patients exhibited 58 differentially expressed proteins (DEPs) and 479 differentially expressed metabolites (DEMs), which might participate in tumour progression and metastasis. Moreover, 75 DEPs were identified among the HC, LC, and LC-T groups. Forty-eight highly expressed DEPs (eg, programmed death-ligand 1 [PD-L1]) in the LC group were found to be downregulated after thermal ablation. These DEPs had significant impacts on pathways such as angiogenesis, immune checkpoint blockade, and pro-tumour chemotaxis. Metabolites involved in tumour cell survival were associated with these proteins at the expression and functional levels. In contrast, 19 elevated proteins (eg, interleukin [IL]-6) were identified after thermal ablation. These proteins were mainly associated with inflammatory response pathways (NF- κ B signalling and tumour necrosis factor signalling) and immune cell activation.

Conclusions Thermal ablation-induced changes in the host plasma microenvironment contribute to anti-tumour immunity in NSCLC, offering new insights into tumour ablation combined with immunotherapy.

[†]Xinglu Zhang and Shuai Shao have authors contributed equally to this work and share first authorship.

*Correspondence:

Zhaohui Tong
tongzhaohuicy@sina.com
Feng Wang
tad2008@hotmail.com
Jieqiong Li
jieqiongli2010@163.com

Full list of author information is available at the end of the article



Trial registration This study was registered on the Chinese Clinical Trial Registry (<https://www.chictr.org.cn/index.html>). ID: ChiCTR2300076517. Registration Date: 2023-10-11.

Keywords Lung cancer, Thermal ablation, Proteomic, Metabolomic, Immune response

Introduction

Lung cancer (LC) is the second most prevalent cancer worldwide and the leading cause of cancer-related deaths, according to GLOBOCAN 2020 estimates of cancer incidence and mortality [1]. Histologically, non-small cell lung cancer (NSCLC) is the most common pathological type of LC, comprising approximately 85% of cases [2]. Despite considerable advances in anti-tumour drugs and immunotherapy in recent years, the 5-year survival rate is low (25.4%) [3]. Surgical resection is generally recommended for patients with early-stage NSCLC. However, more than 15% of patients with stage I or II NSCLC and 30% of patients aged >75 years are considered ineligible for curative surgery [4].

Thermal ablation, which encompasses techniques such as radiofrequency ablation, microwave ablation, and cryotherapy, is a minimally invasive therapeutic approach. Of these, the first two techniques rely on focal tissue heating to denature proteins and dissolve lipids in tumour cells. In contrast, cryoablation involves the application of low temperatures to the targeted tissue, resulting in necrosis of the tumour cells. Thermal ablation has been used in the treatment of various tumours [5–7]. Because it can preserve maximal pulmonary function, thermal ablation is considered a safe and effective modality for controlling unresectable lung tumours, with the potential for high patient survival [8–10]. However, thermal ablation can cause a peripheral immune response by inducing an inflammatory response and tumour-associated antigen release. The various outcomes of thermal ablation depend on diverse factors including interactions between tumour damage and micromolecules, as well as the balance between beneficial and detrimental host immune responses. Yang et al. showed that thermal ablation could slightly inhibit cellular immunity, thereby affecting anti-tumour immunity [11]. Recently, there has been increasing interest in performing thermal ablation with immunotherapy to enhance anti-tumour effects [12–14]. The effect of thermal ablation on the internal microenvironment may be directly associated with patient prognosis. Thus far, changes in the host microenvironment after thermal ablation are not fully understood.

Blood is an ecological information bank that comprises complicated and highly coordinated interactions among diverse molecules, including proteins and metabolites. Multi-omics analysis of molecular interactions in blood has helped to elucidate internal conditions after

treatment. He et al. conducted metabolomics at distinct time points to determine whether metabolic alterations are corrected by curative surgery [15]. Wu et al. utilised a multi-omics approach to investigate the effects of local cryoablation on the distal tumour microenvironment, providing a theoretical basis for cryoablation in combination with other immunotherapy regimens [16]. Dong et al. performed liquid chromatography–mass spectrometry (LC–MS)-based metabolomic analysis of serum samples, combined with 16S rRNA analysis using the Illumina MiSeq platform, to explore the safety and feasibility of nsPEF application in porcine livers [17]. Notably, plasma small molecules can reflect changes in the host after surgical intervention, providing important data to guide treatment planning. To our knowledge, most data concerning thermal ablation-induced immune responses have been derived from studies of mouse peripheral blood samples. Comprehensive analyses of human plasma samples are needed for the translation of thermal ablation to NSCLC treatment.

Here, we performed plasma proteomics and metabolomics analyses of NSCLC patients before and after thermal ablation during the perioperative period; we examined whether proteomic and metabolic alterations were corrected by curative surgery. Additionally, we sought to identify molecular indicators of better therapeutic responses to thermal ablation. The findings may provide useful insights for the development of novel combination therapies.

Methods

Patients and procedures

From February 2023 to January 2024, 136 patients with pulmonary ground-glass nodules were admitted to Beijing Chaoyang Hospital; among these patients, 48 individuals were recruited for this study (Chinese Clinical Trial Registry, ID: ChiCTR2300076517). Patient inclusion criteria were pathological and imaging evidence of NSCLC; multicentric primary NSCLC, or the presence of comorbidities ineligible for surgery; refusal to undergo surgery or other local treatment (eg, stereotactic body radiotherapy); and never received any anti-tumour chemotherapeutic agents or immunotherapy. Thirty-two healthy controls (HCs) were recruited from volunteers who underwent medical examinations at Beijing Chaoyang Hospital during the study period. All patients in this

study provided written informed consent before thermal ablation.

Microwave ablation was performed in our operating room by two pulmonologists with 4 and 5 years of experience. Electromagnetic navigation bronchoscopy (ENB) guidance was used when the chest computed tomography (CT) image showed a clear small airway through or near the nodule or closer to the central area. Otherwise, percutaneous CT guidance was used when the chest CT image showed nodules near the peripheral 1/3 zone of the lung, or when there was no small airway through or near the tumour. Considering nodule location and distance from small airways, 36 patients underwent CT-guided percutaneous microwave ablation, and 12 patients underwent ENB-guided microwave ablation therapy.

During CT-guided percutaneous microwave ablation, the patient was positioned according to the pre-determined puncture path, and a positioning fence was placed. A standard chest CT scan was performed to determine the puncture plane. The puncture site was determined using the fence grid. When the tumour location had been determined, the corresponding area of the body surface was prepared and sterilised. The patient was administered local anaesthesia via pleural surface injection of 2% lidocaine. When the needle reached the lesion, ablation was performed for 6–9 min at a power of 40–60 W, depending on lesion size. The microwave system used a 2450 MHz generator and a 1.1 cm straight antenna. Upon completion of ablation, a CT scan of the whole chest was performed to detect any postoperative complications, such as pneumothorax or bleeding. The target ablation margin was at least 5 mm of normal tissue surrounding each nodule.

Before ENB-guided microwave ablation, a virtual bronchial image was created using a preoperative thin-slice CT reconstruction of the patient's chest. Nodules on the CT image were regarded as targets, and airways were identified by labelling on the corresponding virtual bronchial tree images. All procedures were performed using a single-lumen endotracheal tube or laryngeal mask airway involving a flexible bronchoscope (BF-UC260FW, Olympus). Patients were placed under general anaesthesia and an anaesthesiologist was present throughout the ablation procedure. A bronchial navigation system (Archimedes System, Broncus Medical, Inc., San Jose, CA, USA) was utilised to accurately locate the pulmonary lesion. When the peripheral catheter had reached the lesion site, a flexible microwave antenna (MTC-3CA-II6/Φ1.8 mm; Vison-China Medical Devices R&D Center), which was water-cooled and coupled to a microwave platform, was inserted into the tumour through the peripheral catheter. Based on our experience, treatments were generally performed using 40–60 W power for 5–10 min. When

necessary, repeat ablation was performed using a different route to ensure better tumour coverage. Upon completion of ablation, a CT scan of the entire chest was performed to determine extent of ablation and detect any postoperative complications. Oxygen administration and electrocardiogram monitoring were performed throughout the procedure.

Blood samples collection and processing

To isolate plasma, peripheral venous blood samples (2 mL/ethylenediaminetetraacetic acid [EDTA] tube) were collected from each patient at two time points. The first baseline sample (LC) was collected before ablation, and a second sample (LC-T) was collected 24 h after ablation. All blood samples were centrifuged at 2000×g for 20 min at 4 °C. Plasma was then separated, flash-frozen in liquid nitrogen, and stored at –80 °C until multi-omics analysis. Additionally, plasma samples from 32 HCs were processed and stored in the same manner.

Olink proteomics analysis

The Olink® Target 96 immuno-oncology proteomics platform (Olink® Bioscience, Sweden) was used to analyse EDTA plasma samples. This platform can simultaneously assess 92 specific immuno-oncology-related proteins using 1 µL of each sample (Supplementary Table 1). The platform uses a proximity extension assay methodology combined with next-generation sequencing output to accurately quantify the amounts of 92 proteins in each sample. The primary outputs were Cq values (quantification cycle number) corresponding to each protein. These Cq values were normalised and presented in the form of normalised protein expression (NPX) units on a logarithmic scale. Higher NPX values correspond to higher protein expression. The entire experimental procedure was monitored by four internal controls, including two incubation/immunisation controls (non-human antigen and antibody pair), an extension control (IgG antibody and matching probes), and a detection control (a complete double-stranded amplicon). Additionally, eight external controls were utilised to ensure quality control (QC) and to normalise the data. The external controls comprised two sample controls (to estimate precision between batches), three negative controls (to detect background signals), and three inter-plate controls (to normalise data). The quality of each sample was assessed by calculating the standard deviations of the detection and incubation/immunisation controls. The NPX values of the incubation/immunisation controls and detection controls for each sample were within a range of ±0.3 NPX from the median of the run. Samples with deviations >0.3 NPX did not meet the QC criteria.

Metabolomic analysis

Samples were removed from -80°C storage and defrosted at room temperature. For each sample, 100 μL were placed in a 1.5-mL Eppendorf tube containing 400 μL of a chilled solution comprising methanol and acetonitrile (1:1 volume ratio). The mixtures were agitated using a vortex mixer for 1 min. Subsequently, samples were subjected to ultrasonic extraction in an ice water bath for 10 min. Finally, the samples were stored at -20°C for 60 min. The resulting extracts were centrifuged at 13,000 rpm for 10 min at 4°C . The supernatants (100 μL each) were lyophilised in glass vials using a centrifugal dryer. Next, each sample was supplemented with 200 μL of water and methanol (4:1 volume ratio). The samples were vortexed for 30 s, subjected to ultrasonic extraction for 3 min in an ice water bath, and then stored at -20°C for 2 h. Subsequently, the samples were centrifuged at 13,000 rpm for 10 min at 4°C . The supernatant in each tube was extracted using a crystal syringe, passed through a 0.22- μm microfilter, and transferred to a vial. Processed samples were stored at -80°C until LC-MS analysis. Pooled QC samples were prepared by combining small volumes of all experimental samples.

High-performance liquid chromatography (ACQUITY UPLC I-Class plus) was performed in this study. Target chemicals were separated by liquid chromatography on a chromatographic column (ACQUITY UPLC HSS T3; 100 mm \times 2.1 mm, particle size: 1.8 μm). Under full-loop injection mode, a 5- μL injected sample volume was used for each run. The mobile phase had a flow rate of 0.35 mL per minute. Gradient elution was conducted using mobile phase A (water containing 0.1% formic acid) and mobile phase B (acetonitrile containing 0.1% formic acid). Mass spectrometry experiments were performed with the Thermo-Q-Exactive instrument. Measurements were collected in both positive and negative V-geometry modes. The spray voltages were set to 3800 V and -3000 V, respectively. Other parameters were established as follows: capillary temperature, 320°C ; sheath gas flow rate, 35 Arb; aux gas flow rate, 8 Arb; full MS resolution, 70,000; MS/MS resolution, 17500; and collision energy, 10/20/40.

Statistical analysis of multi-omics data

Raw LC-MS data were analysed using Progenesis QI v3.0 software (Nonlinear Dynamics, Newcastle, UK) for peak detection, baseline filtration, retention time correction, and peak alignment and normalisation. Proteins and metabolites were compared between the two groups using two-tailed Student's *t*-tests, and *P*-values were adjusted by Benjamini-Hochberg correction (adjust $P < 0.05$). Statistical significance in multigroup analyses was calculated by one-way analysis of variance and

Tukey's honestly significant difference test. Fold change (FC) values were calculated to compare each pair of groups. Compounds exhibiting FC values > 1.5 or < 0.67 ($P < 0.05$) were considered significantly different between the two groups. Compound identification relied on accurate determination of the mass-to-charge ratio (*M/z*), studies of secondary fragments, and assessments of isotopic distribution; these qualitative analyses were performed on the Human Metabolome Database (HMDB), Lipidmaps (V2.3), and Metlin databases.

Differentially expressed proteins (DEPs) and differentially expressed metabolites (DEMs) were depicted using volcano plots and heatmaps. Partial least squares-discriminant analysis (PLS-DA) of omics data was conducted on the BioDeep Platform (<https://www.biodeep.cn>). Multi Experiment Viewer software (MeV, version 4.7.4) was used to display heatmaps. Signalling pathway analysis was conducted with the Kyoto Encyclopedia of Genes and Genome (KEGG) database (<https://www.kegg.jp/kegg/>). Volcano plots were established using a combination of FC and *t*-tests.

Results

Baseline characteristics

We first compared baseline data between LC patients and HCs. In total, 80 individuals (48 LC patients and 32 HCs) were included in this study. Olink proteomics and untargeted metabolomics were performed to establish a comprehensive molecular landscape of the LC patients (Fig. 1). The patient characteristics are displayed in Table 1. There were no statistically significant differences between LC patients and HCs in terms of age, sex, smoking history, and comorbidities ($P > 0.05$). Among LC patients, the mean tumour size was 11.7 ± 4.5 mm and most tumours (93.7%) were adenocarcinomas. Tumour staging was determined to be at an early stage in all patients, including those with adenocarcinoma in situ and stage T1. Approximately 75% of the patients were treated with CT-guided percutaneous microwave ablation, whereas 25% of the patients were treated with ENB-guided microwave ablation; these treatments were dependent on the locations of lung nodules.

Omics profiling of LC patients

Elevated cancer-related proteins in LC patients

Using the Olink immuno-oncology proteomics platform, we detected 92 pre-specified proteins in plasma samples from LC patients and HCs (Supplementary Table 2.1). A boxplot of Olink proteomics data (Figure S1a) was generated to confirm validity. PLS-DA revealed a clear distinction between LC patients and HCs (Fig. 2a). The comparison revealed 58 DEPs between the LC and HC groups. As shown in Fig. 2b,

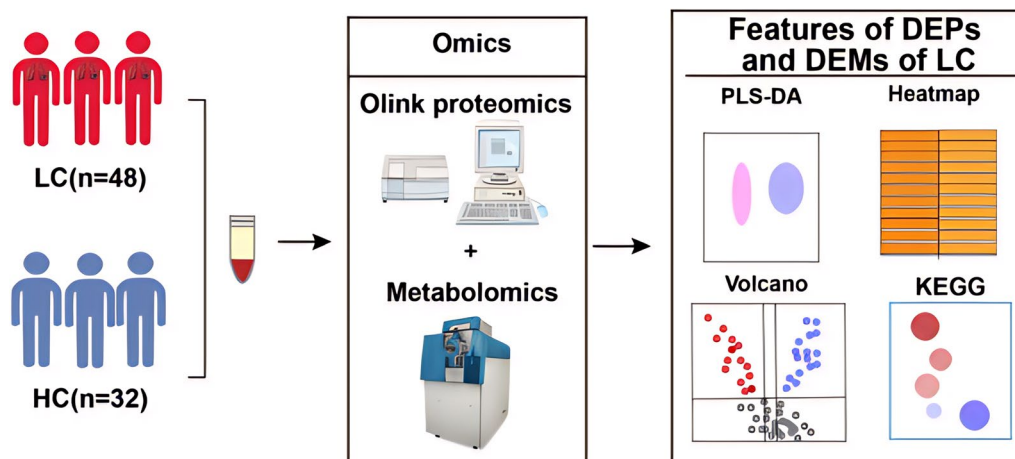


Fig. 1 Study overview. Eighty individuals including 48 lung cancer patients and 32 HCs were recruited. Plasma samples were collected from each participant for Olink proteomics and metabolomics to identify lung cancer-related DEPs and DEMs

Table 1 Summary of participant demographics and tumour characteristics at baseline

Variable	Lung cancers (n = 48)	Healthy controls (n = 32)	P value
Age(yr)			
Mean \pm SD	65.5 \pm 7.6	65.6 \pm 8.1	0.921
\geq 65	32(66.7%)	20(62.5%)	0.702
< 65	16(33.3%)	12(37.5%)	
Gender			
Male	19(39.6%)	15(46.9%)	0.518
Female	29(60.4%)	17(53.1%)	
Smoking history			
Yes	22(45.8%)	13(40.6%)	0.645
No	26(54.2%)	19(59.4%)	
Comorbidities			
Hypertension	19(39.6%)	9(28.1%)	0.853
Diabetes Mellitus	10(20.8%)	6(18.8%)	
Coronary heart disease or PCI	8(16.7%)	3(9.4%)	
Tumor size(mm)	11.7 \pm 4.5	–	/
Histology			
Adenocarcinoma	45(93.7%)	–	/
Squamous cell carcinoma	3(6.3%)	–	/
Stage			
TisNOM0	2(4.2%)	–	/
T1aNOM0	18(37.5%)	–	/
T1bNOM0	25(52.1%)	–	/
T1cNOM0	3(6.2%)	–	/
Ablation pathway			
CT-guided percutaneous microwave ablation	36(75.0%)	–	/
ENB-guided microwave ablation	12(25.0%)	–	/
Total ablation time (min)	8.0 \pm 1.2	–	/

SD Standard deviation, PCI Percutaneous coronary intervention, CT Computed tomography, ENB Electromagnetic navigation bronchoscope

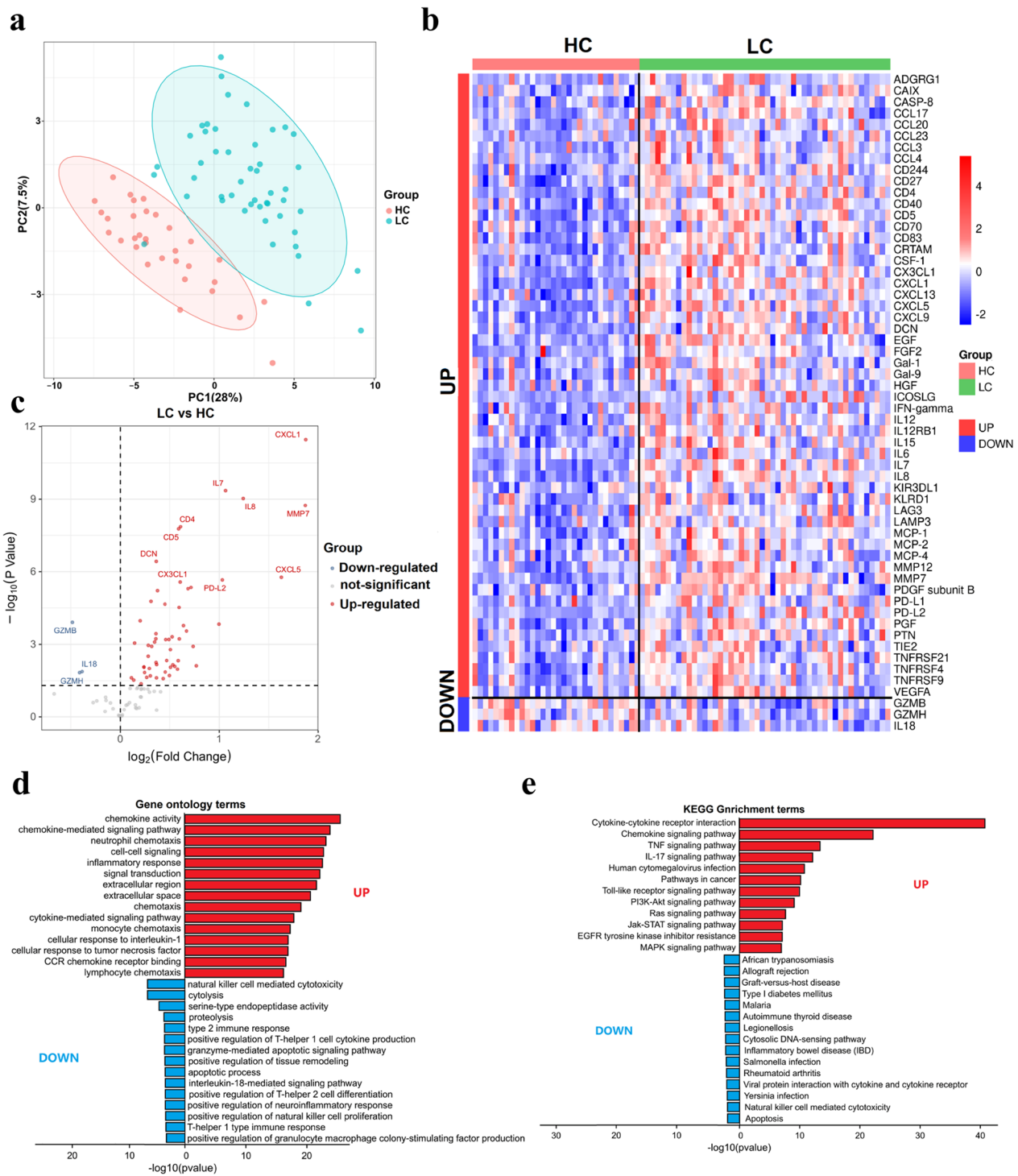


Fig. 2 Altered cancer-related proteins in LC patients. **a** PLS-DA score plots of differentially expressed proteins (DEPs) in HC and LC groups. **b** Heatmap of DEPs between HC and LC groups (FC > 1.5 or < 0.67, adjust P < 0.05). **c** Volcano plot showing the top 10 upregulated and downregulated proteins with the greatest differences between HC and LC groups. **d** GO analysis of DEPs between HC and LC groups. **e** KEGG analysis of DEPs between HC and LC groups. Top pathways are shown in this figure

most DEPs (55/58, 94.8%) exhibited greater expression in the LC group than in the HC group. The top 10 upregulated proteins with the greatest differences were CXCL-1, IL-7, IL-8, MMP7, CD4, CD5, DCN, CXCL5, PD-L2, and CX3CL1 (Fig. 2c). GO analysis and KEGG pathway enrichment analysis were performed with a focus on these DEPs. The GO analysis (Fig. 2d) demonstrated enrichment in processes related to cell chemotaxis and signal transduction, whereas KEGG enrichment analysis (Fig. 2e) indicated that tumour-related signalling pathways were upregulated. Furthermore, the GO analysis and KEGG enrichment analysis showed that natural killer cell-mediated cytotoxicity was downregulated, which could promote tumour immune escape and metastasis [18]. Collectively, these results indicated that the elevated plasma proteins are mainly involved in intercellular chemotaxis and signal transduction, with important implications in tumour progression and metastasis.

Disturbed metabolism in LC

In parallel, we conducted a metabolomics analysis and identified a total of 3459 metabolites. A boxplot of metabolomics data (Figure S1b) was generated to confirm validity. PLS-DA (Fig. 3a) was performed to compare metabolite expression between LC and HC groups. Overall, 479 DEMs were identified between HC and LC groups based on FC values >1.5 or <0.67 ($P < 0.05$) (Fig. 3b). Of these 479 DEMs, 229 were upregulated and 250 were downregulated in LC patients compared with HCs (Fig. 3c, Supplementary Table 2.2). Intriguingly, we found that the up- and downregulated DEMs exhibited distinct hierarchical clustering between the two groups (Fig. 3b). DEMs related to amino acids, azoles, fatty acyls, glycerolipids, and glycerophospholipids were all substantially decreased in LC patients compared with HCs. Conversely, DEMs related to prenol lipids, purines, pyrimidines, sphingolipids, steroids, and steroid derivatives were considerably increased in LC patients compared with HCs. Moreover, we found that the upregulated DEMs were enriched in tumour-associated metabolic pathways such as primary bile acid biosynthesis [19], arginine and proline metabolism [20, 21], purine metabolism [22], and folate biosynthesis [23], consistent with previous studies. In contrast, the linoleic acid metabolism pathway, reportedly associated with anti-tumour effects [24], was significantly suppressed because DEMs in this pathway were decreased in LC patients compared with HCs (Fig. 3d). Overall, our findings of metabolic dysfunction in LC patients are consistent with the results of previous plasma metabolomics studies.

Significant changes in plasma proteins and metabolites among LC patients after thermal ablation

Thermal ablation is a minimally invasive therapeutic technique that utilises focal tissue heating for tumour treatment. To assess the effectiveness and safety of this procedure, we collected plasma from patients before (LC) and 24 h after (LC-T) thermal ablation to explore its effects via proteomics and metabolomics (Fig. 4a). The raw data of patients and controls were shown in Table S3.

As shown in Fig. 4b, there was a clear distinction between LC patients and HCs; there was also a significant difference between LC and LC-T groups. In total, 75 DEPs were identified among the three groups (Fig. 4c). There were 43 DEPs (31 decreased and 12 increased) between the LC and LC-T groups (Supplementary Table 2.1). Our results implied that most altered proteins tended to slightly return to healthy levels after thermal ablation.

As an assessment of the overall associations between biochemical parameters and outcomes, we utilised redundancy analysis to clarify how explanatory variables influenced differences among the three groups. As shown in Fig. 4d, redundancy analysis revealed a clear correlation of the LC group with higher levels of cell migration-related proteins (ANGPT1, TIE2, EGF, CXCL5, CCL17, ADA) and cell adhesion-related proteins (CD5, LAG3, TNFRSF21). Three expression patterns including an inverted “V” cluster (cluster 1), an increasing cluster (cluster 2), and a decreasing cluster (cluster 3) were observed across the different groups (Fig. 4e). Taken together, these findings suggested that thermal ablation could repair damage to the microenvironment, highlighting possible therapeutic roles for such proteins.

Metabolomic changes induced by thermal ablation

We also explored whether thermal ablation affected plasma metabolism. To determine the metabolomic effects of thermal ablation, we utilised untargeted metabolomics for analysis of DEMs in the plasma of LC patients before and after treatment (Supplementary Table 2.2). PLS-DA (Figure S2a) and a Venn diagram (Figure S2b) highlighted DEMs identified in each pairwise comparison. These DEMs were then depicted in heatmap format to show the effects of thermal ablation on LC patients. Next, we examined expression patterns (Figure S3a) and conducted KEGG analysis (Figure S3b) to facilitate further correlation studies.

Reduced cancer indicators and related tumour activity pathways after thermal ablation

Multiple studies have revealed that tumour patients display substantial differences in tumour-associated

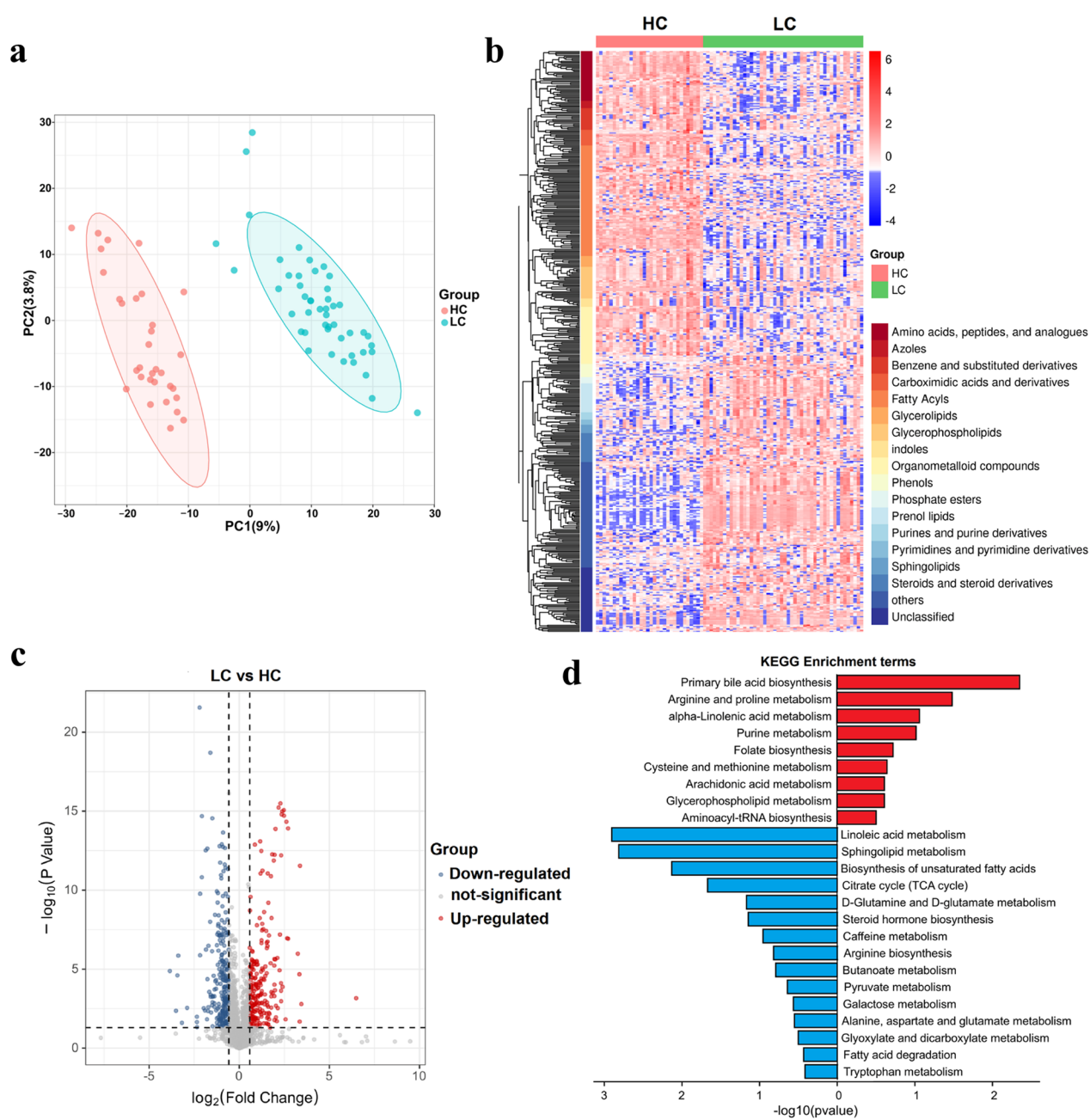


Fig. 3 Altered cancer-specific metabolites in LC patients. **a** PLS-DA score plots of differentially expressed metabolites (DEMs) in HC and LC groups. **b** Heatmap of DEMs between HC and LC groups ($FC > 1.5$ or < 0.67 , $\text{adjust } P < 0.05$). **c** Volcano plot showing 229 upregulated DEMs and 250 downregulated DEMs in LC patients compared with HCs. **d** KEGG enrichment analysis of DEMs between HC and LC groups

signalling pathways after thermal ablation [25]; however, the mechanisms underlying these differences, especially in human samples, remain unclear. It is also unclear how metabolites, key factors in the regulation of such pathways and production of required components, are involved in these processes. To address these

uncertainties, we analysed DEPs from inverted “V” cluster (cluster 1).

As shown in Fig. 5a, 48 DEPs with high expression in the LC group showed a decreasing trend in plasma collected at 24 h after thermal ablation. For example, we observed that the levels of CXCL11 and CXCL5, with

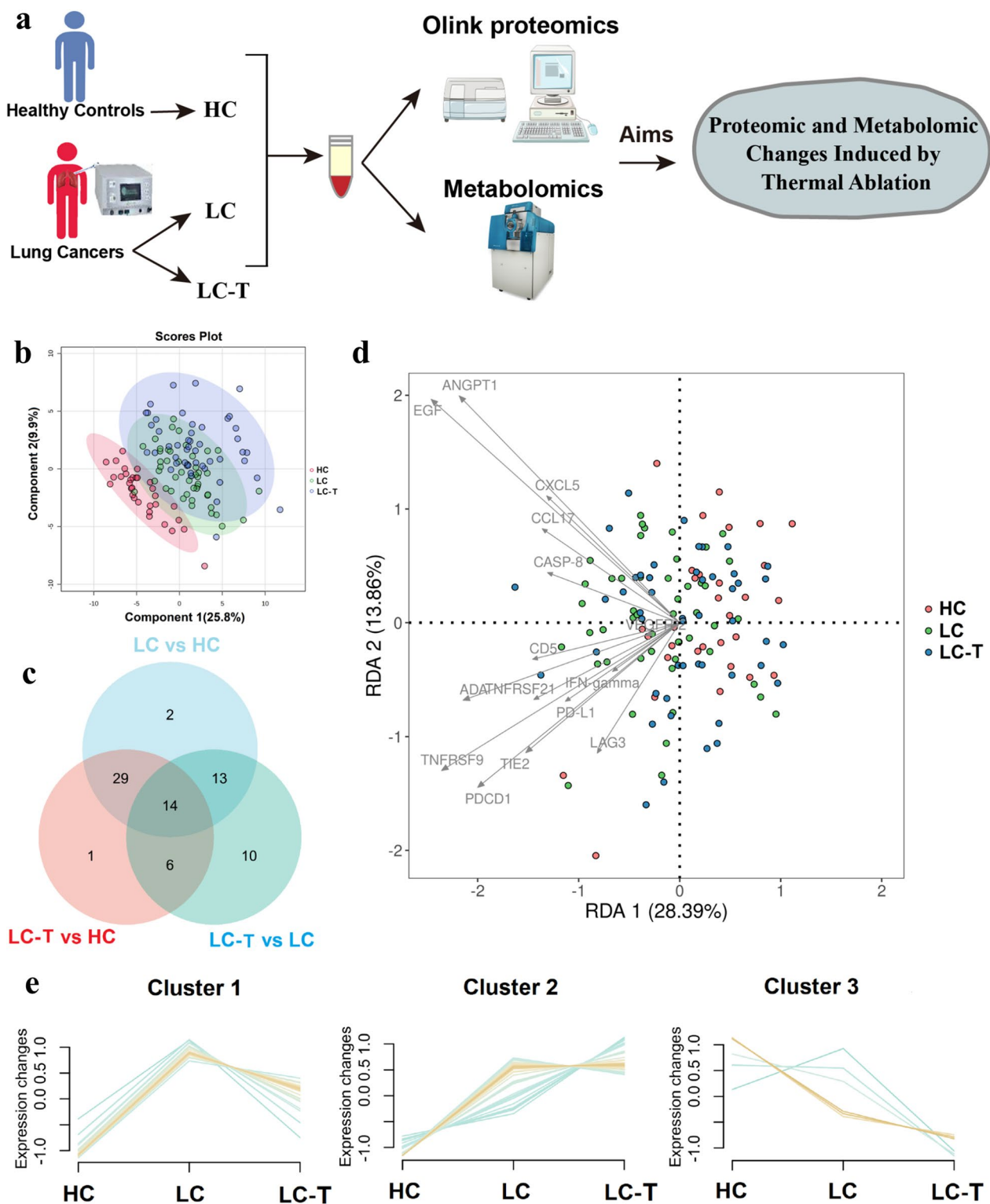


Fig. 4 Landscapes of differentially expressed proteins (DEPs) among HC, LC, and LC-T groups. **a** Study overview. Plasma samples were collected from lung cancer patients at 24 h after thermal ablation, then subjected to Olink proteomic and metabolomic analyses to construct an integrated network. **b** PLS-DA score plots of DEPs in HC, LC, and LC-T groups. **c** Venn diagram showing the number of DEPs in each group. **d** Redundancy analysis plot showing explanatory variables that contributed to differences among the three groups. **e** Hierarchical clustering illustrating three DEP patterns across the three groups. Each line in the figure represents a protein, and the orange line represents the mean expression level of all proteins

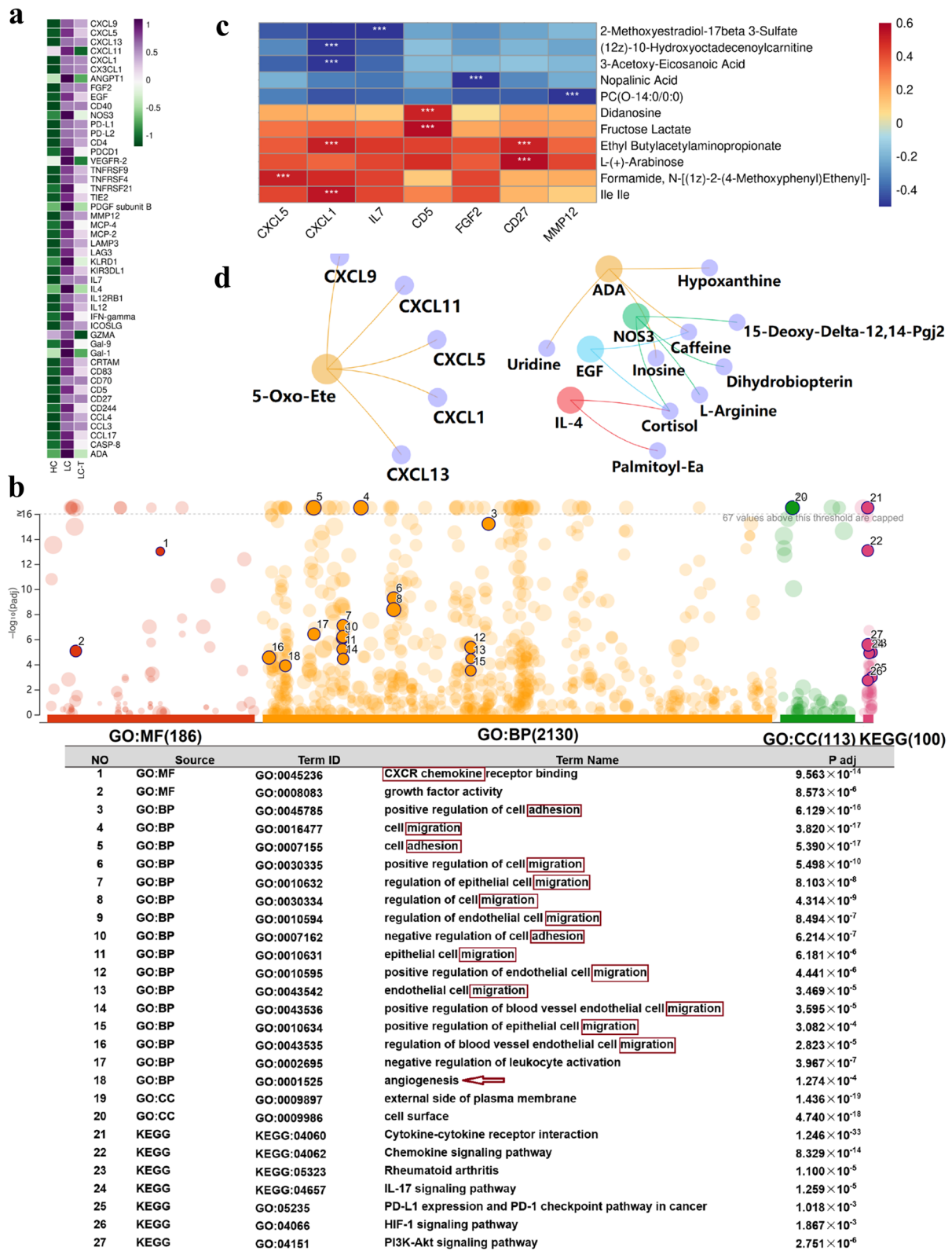


Fig. 5 Reduced cancer indicators and related pathways after thermal ablation. **a** Heatmap of 48 decreased DEPs after ablation among the three groups. The two columns show the fold change (FC) values of DEPs in each cohort. **b** GO analysis and KEGG enrichment analysis of decreased DEPs after ablation. **c** Spearman correlation analysis of DEPs and DEMs ($R > 0.5$ and $P < 0.05$). **d** Interactions between DEPs and DEMs

roles in fibroblast-directed carcinoma invasion [26], were substantially lower in the LC-T group than in the LC group. Our results implied that some metastatic factors were significantly reduced after surgery. Moreover, CXCL9, CXCL5, CXCL13, CXCL11, CXCL1, and CX3CL1, which have been associated with cell adhesion and cell migration [27], demonstrated an inverted “V” trend after treatment. Similar expression patterns were observed among proteins associated with angiogenesis (CX3CL1, CXCL13, ANGPT1, FGF2, EGF, CD40, and NOS3) and immune checkpoint blockade (PD-L1, EGF, CD4, and PDCD1) (Figure S4).

Intriguingly, based on P -values < 0.05 , analysis of DEPs in cluster 1 revealed that treatment significantly altered CXCR chemokine receptor binding, as well as cell migration and adhesion pathways (Fig. 5b). KEGG enrichment analysis (Fig. 5b) showed that decreased DEPs in the LC-T group were involved in cytokine-mediated signalling ($P = 1.246 \times 10^{-33}$), chemokine signalling ($P = 8.329 \times 10^{-14}$), IL-17 signalling ($P = 1.259 \times 10^{-5}$), PD-L1 expression and PD-1 checkpoint signalling in cancer ($P = 1.018 \times 10^{-3}$), HIF-1 signalling ($P = 1.867 \times 10^{-3}$) and PI3K-Akt signalling ($P = 2.751 \times 10^{-4}$).

Metabolic rewiring and epigenetic remodelling, which are closely linked and exhibit mutual regulation, are well-known hallmarks of cancer [28]. To clarify the roles of metabolites in these recovery processes, we analysed correlations between proteins and metabolites. We used Spearman correlation coefficients to identify significant correlations of DEPs and DEMs ($R > 0.5$ and $P < 0.05$; Fig. 5c). CXCL1, a key factor in chemotaxis, was negatively correlated with 3-acetoxy-eicosanoic acid and (12z)-10-hydroxyoctadecenoylcarnitine; it was positively correlated with ethyl butylacetylaminopropionate, Ile Ile (Fig. 5c). Moreover, downregulated chemokines (CXCL9, CXCL11, CXCL5, CXCL1, and CXCL13) after treatment were closely associated with 5-oxo-6,8,11,14-eicosatetraenoic acid (5-Oxo-ETE), which may inhibit tumour cell survival [29]. Proteins associated with cell migration according to GO analysis (ADA, IL-4, NOS3, and EGF) formed a network that was correlated with various DEMs (Fig. 5d). The correlations of these DEPs and DEMs are shown in Figure S5a. Collectively, these results indicate that correlations emerged between proteomics and metabolomics after thermal ablation, along with decreases in tumour angiogenesis, metastasis and adhesion.

Increased inflammatory factors and immune response proteins after thermal ablation

Furthermore, we identified 19 upregulated DEPs in LC patients after thermal ablation (Fig. 6a). Many of these proteins (IL-6, IL-8, IL-10, IL-15, CCL19,

CCL20, CCL23, PTN, and HGF) were associated with inflammatory responses (Fig. 6a and Figure S6). IL-6 reportedly can induce pro-inflammatory and anti-inflammatory responses in tumour tissue. We observed a gradual increase in IL-6 expression among LC patients after thermal ablation, implying that surgery can partially stimulate local and systemic inflammatory responses. Consistent with this speculation, GO and KEGG analyses indicated that these DEPs were mainly enriched in proteins related to inflammatory response pathways (NF- κ B signalling and tumour necrosis factor signalling) and immune cell activation (eg, T lymphocytes) (Fig. 6b).

In parallel, we conducted Spearman correlation analysis based on the mean normalised quantities of proteins and metabolites. Correlations with $R > 0.5$ and $P < 0.05$ are depicted in Fig. 6c. Among them, IL-6 had the most extensive interactions with DEMs. IL-6 is considered a critical lynchpin between inflammation and cancer [30]. In this study, the expression level of IL-6 was positively correlated with the expression levels of oxotremorine, 5'-methylthioadenosine, fusaric acid, nebracetam, and lidocaine. Moreover, we constructed a gene-metabolite interaction network that enabled the exploration and visualisation of interactions between functionally related metabolites and genes. This network revealed that IL-6 also interacted with fatty acids (15-deoxy-delta-12,14-Pg2, palmitic acid, and eicosapentaenoic acid) and steroid-related metabolites (corticosterone, cortisone, and cortisol) (Fig. 6d). Other correlations between DEPs and DEMs are depicted in Figure S5b. Taken together, these results suggest that thermal ablation leads to upregulation of the inflammatory response and activation of immune cells, such as T lymphocytes. The continuous increase in IL-6 expression might be detrimental, and further research should be conducted to reduce the adverse effects of thermal ablation.

Surgery regulates the systemic status of LC patients

As mentioned above, inflammation-related and tumour-related proteins were elevated in LC patients compared with HCs. After thermal ablation, most proteins (CXCL9, CXCL5, CXCL13, CXCL11, CXCL1, CX3CL1, ANGPT1, FGF2, EGF, CD40, NOS3, and PD-L1) tended to return to normal expression levels. However, some inflammation-related proteins (IL-6, IL-15, CCL23, and HGF) tended to continuously increase after thermal ablation. Collectively, the results indicate that thermal ablation of NSCLC induces an enhanced inflammatory response, accompanied by reductions of tumour-associated proteins and metabolic pathways in plasma (Fig. 7).

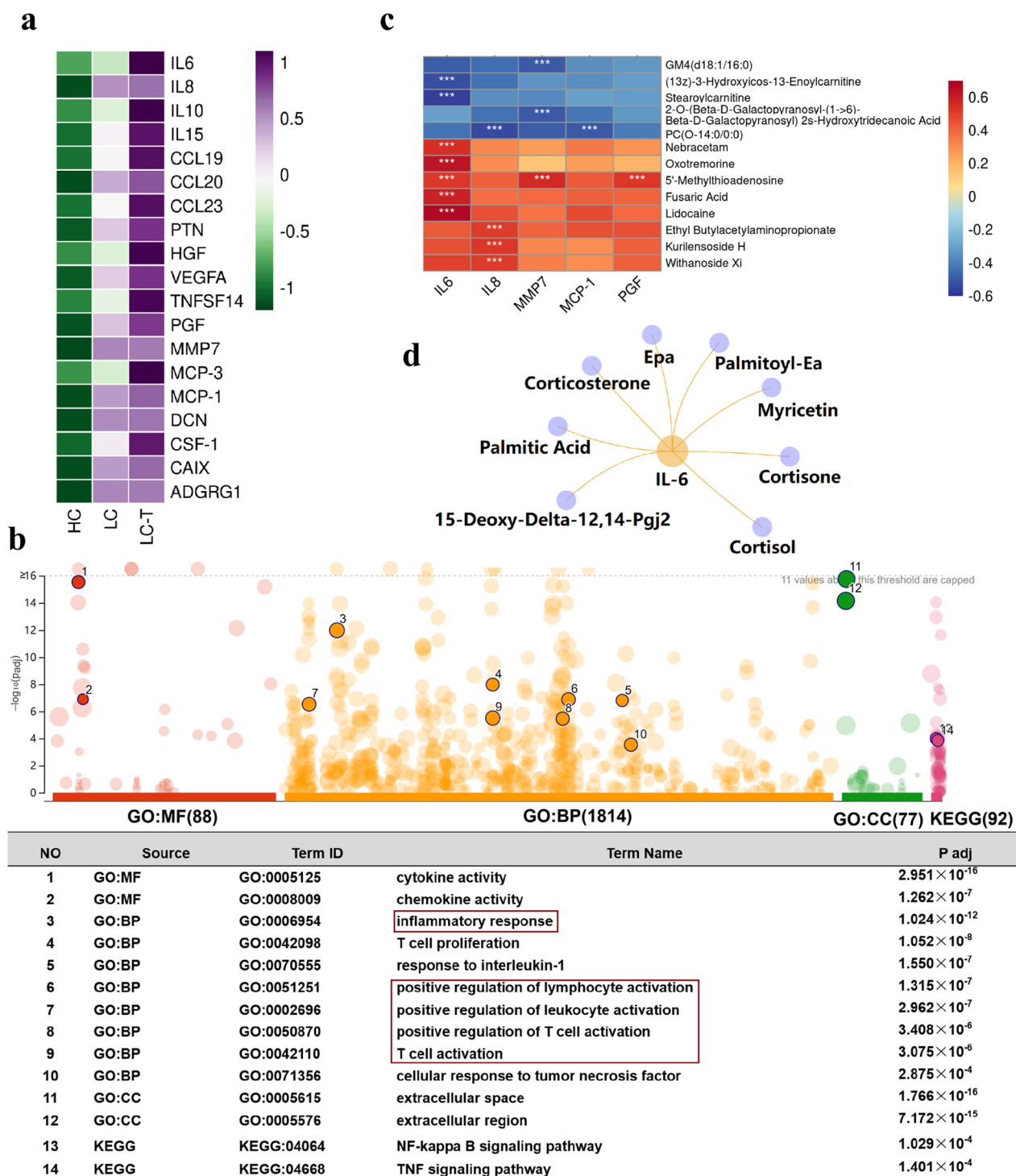


Fig. 6 Increased inflammatory factors and immune response proteins after thermal ablation. **a** Heatmap of 19 elevated DEPs after ablation among the three groups. **b** GO analysis and KEGG enrichment analysis of elevated DEPs after ablation. **c** Spearman correlation analysis of DEPs and DEMs among the HC, LC, and LC-T groups ($R > 0.5$ and $P < 0.05$). **d** Interactions between DEPs and DEMs

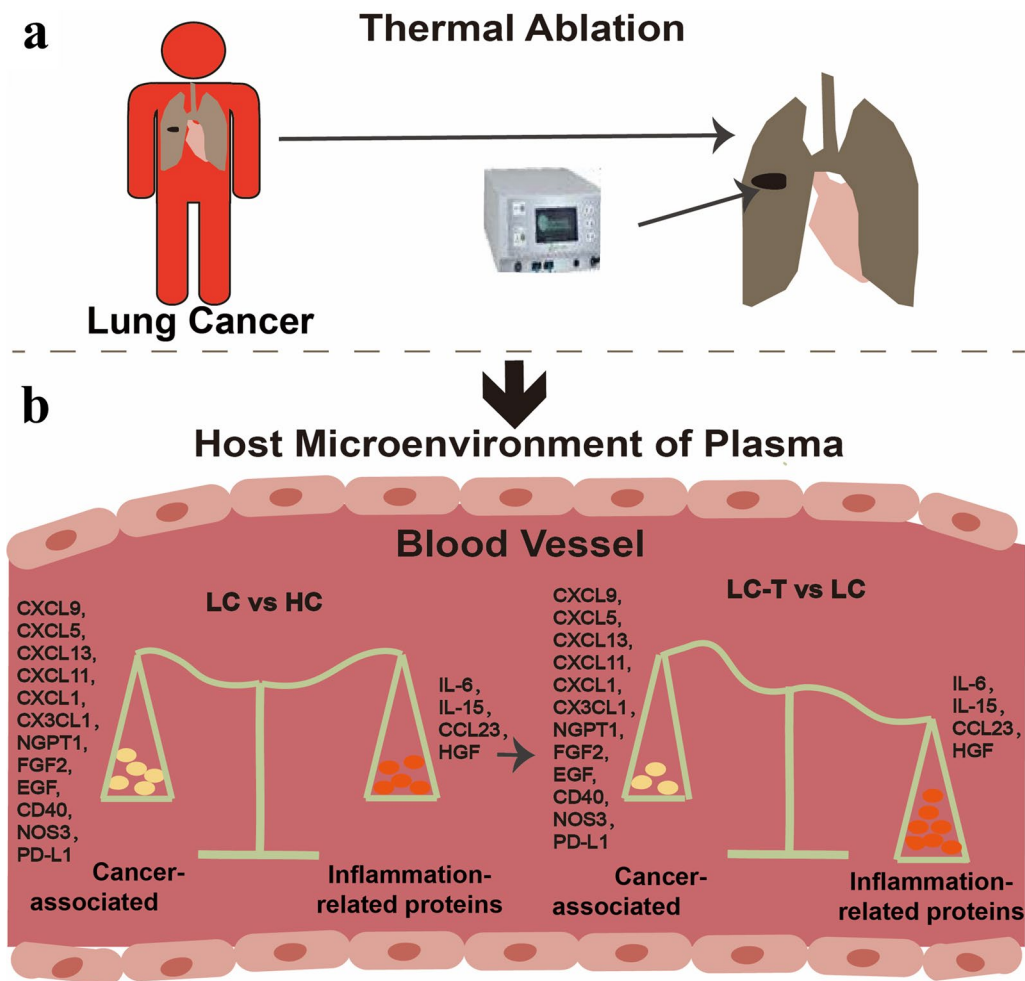


Fig. 7 Thermal ablation regulates the systemic status of LC patients. Changes in the internal microenvironment induced by thermal ablation of lung cancer. Thermal ablation activates the systemic inflammatory response while decreasing the expression levels of pro-tumour protein pathways and metabolic pathways such as angiogenesis, immune checkpoint blockade, and pro-tumour chemotaxis

Short-term efficacy and follow-up of thermal ablation for NSCLC

In this study, all 48 patients successfully located pulmonary nodules and completed the ablation of the target zone. There were no deaths related to the procedure. Some patients experienced complications, including 16(33.3%) cases of pneumothorax, 7(14.6%) cases of pleural effusion, and 2(4.2%) cases of haemoptysis. Patients with pneumothorax were managed with chest drainage. None of the patients with pleural effusion required tube drainage, and it could be absorbed on its own. Two patients developed bloody sputum after ablation, and no hemoptysis occurred. The diameter of the lesions observed by chest CT scan on days 1, 30, and

Table 2 Short-term efficacy and follow-up of thermal ablation for NSCLC

Variables	NSCLC(n = 48)
Postoperative complications	
Pneumothorax	16(33.3%)
Pleural effusion	7(14.6%)
Bloody sputum	2(4.2%)
Technical success rate	48(100%)
CT imaging findings of the lesion	
24 h Postoperative	26.1±8.9
1 month Postoperative	18.0±7.0
3 months Postoperative	11.8±5.9

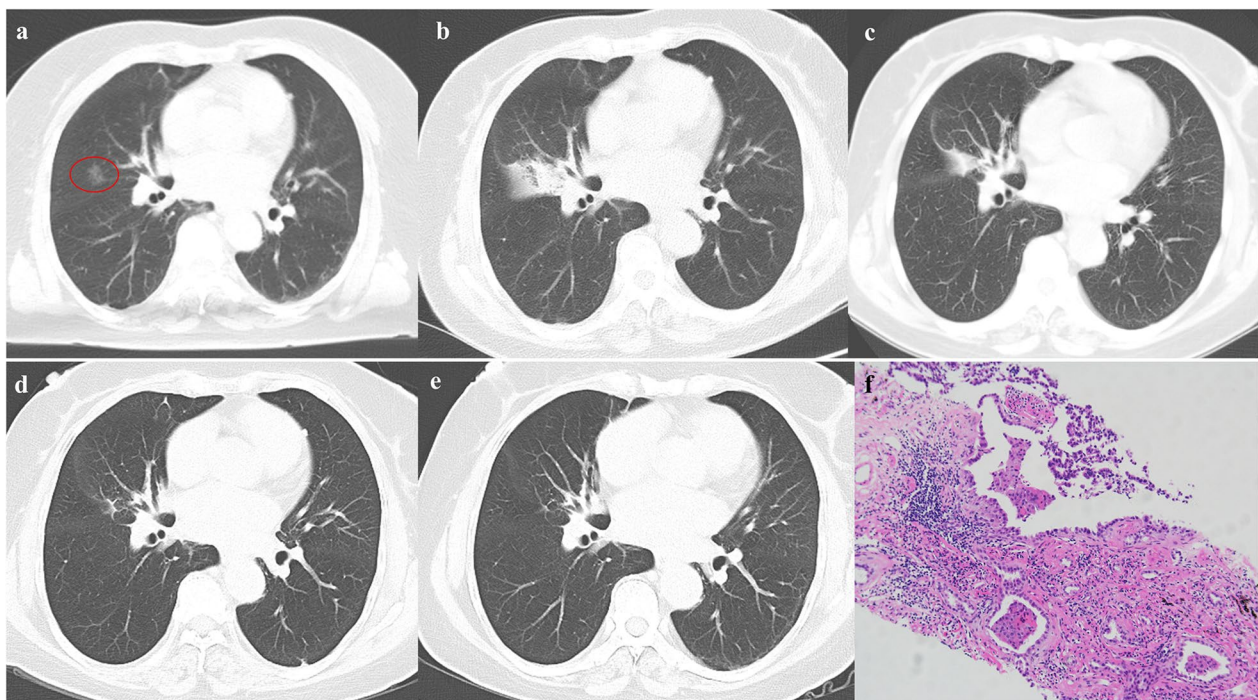


Fig. 8 Chest CT images of ENB-guided microwave ablation for non-small cell lung cancer, including images taken before, after, and during follow-up. **a** Chest CT imaging demonstrated the presence of a ground glass nodule in the middle lobe of the right lung, with an approximate size of 9 mm × 11 mm. **b** Chest CT image conducted 24 h after ENB-guided microwave ablation. **c** A follow-up chest CT scan was conducted one month after thermal ablation, demonstrating a reduction in the size of the ablated focal scar. **d–e** The sustained reduction of the ablated zone on follow-up chest CT at 3 months and 6 months post-thermal ablation, respectively. **f** The pathological diagnosis of adenocarcinoma in situ prior to thermal ablation

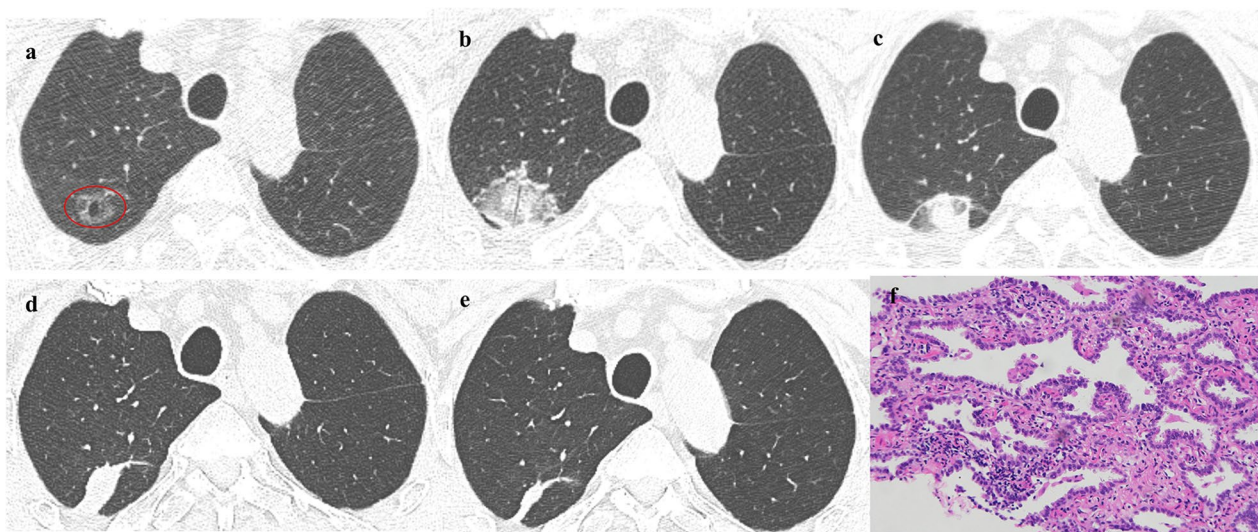


Fig. 9 Chest CT images of CT-guided percutaneous microwave ablation for non-small cell lung cancer, including images taken before, after, and during follow-up. **a** Chest CT imaging revealed the presence of a ground glass nodule in the upper lobe of the right lung, with an approximate size of 10 mm × 12 mm. **b** Chest CT image obtained 24 h after percutaneous microwave ablation. **c** A follow-up chest CT scan was conducted one month after thermal ablation, demonstrating a reduction in the size of the ablated focal scar. **d–e** The sustained reduction of the ablated zone on follow-up chest CT at 3 months and 6 months post-thermal ablation, respectively. **f** The pathological diagnosis of adenocarcinoma

90 after ablation were 26.1 ± 8.9 mm, 18.0 ± 7.0 mm, and 11.8 ± 5.9 mm, respectively (Table 2). Figures 8 and 9 illustrated typical thermal ablation cases of ENB-guided and CT-guided percutaneous microwave ablation, respectively. Due to the limited follow-up period, no statistical analysis of progression-free survival or overall survival was conducted in this group of cases.

Discussion

Thermal ablation, a minimally invasive treatment for NSCLC, spares the lung parenchyma and preserves maximum pulmonary function. This treatment has been endorsed by multiple professional societies [31–33]. The heat generated during thermal ablation causes tumour cell necrosis, destroying the tumour. Current indications for lung thermal ablation therapy include multifocal primary NSCLC, pulmonary metastases, and pain palliation of chest wall tumours [34]. Thus far, most evaluations of the safety and efficacy of thermal ablation in NSCLC have focused on clinical trials; the underlying thermal ablation-induced changes in the host microenvironment are unknown. To address this lack of information, we utilised Olink proteomics and metabolomics to investigate thermal ablation-induced changes in plasma proteins and metabolites. To our knowledge, this is the first study to combine proteomic and metabolomic data from NSCLC patients undergoing thermal ablation.

We observed significant differences in plasma proteins and metabolism between LC patients and HCs. Next, we conducted integrated proteomic and metabolomic analyses of plasma samples from NSCLC patients before and after thermal ablation, as well as HCs. These analyses showed that the expression levels of pro-tumour proteins and metabolic pathways (eg, angiogenesis, immune checkpoint blockade, and pro-tumour chemotaxis) were downregulated. Angiogenesis is a complex and tightly regulated process that promotes tumour growth, invasion, and metastasis in LC and other malignancies. Multiple angiogenic factors and receptors are involved in this process; many of them function in a synergistic manner. For example, angiopoietin 1 (ANGPT1) is a secreted factor that regulates angiogenesis via binding to the endothelial cell-specific receptor tyrosine kinase TIE2, which promotes blood vessel maturation and stabilisation [35]. Additionally, an animal study showed that simultaneous overexpression of platelet-derived growth factor subunit B (PDGF-BB) and FGF2 in murine fibrosarcoma led to the formation of high-density primitive vascular plexuses. PDGF-BB and FGF2 mutually enhance endothelial and mural cell responses, leading to disorganised neovascularisation and metastasis [36]. In the present study, we found that the expression levels of these interacting angiogenic factors (ANGPT1,

TIE2 and EGF2) were decreased at 24 h after ablation. Similar expression trends have been observed for other angiogenic molecules, including EGF [37] and NOS3 [38]. Therefore, thermal ablation may exert a protective function by inhibiting neovascularisation, suppressing tumour metastasis.

Despite substantial progress regarding immune checkpoint blockade therapy for tumours in recent years, some challenges remain, such as the immunosuppressive tumour microenvironment and the lack of known tumour-associated antigens [25]. A clinical study of advanced hepatocellular carcinoma demonstrated that thermal ablation increased the objective response rate with tolerable toxicity and achieved better median survival during anti-PD-1 therapy [39]. Additionally, a previous animal study showed that ablation and PD-1 blockade therapy had synergistic anti-tumour effects [40]. The present study showed that the PD-L1 expression and PD-1 checkpoint pathways were downregulated in NSCLC patients at 24 h after thermal ablation. PD-1 is regarded as a co-inhibitory receptor that suppresses T-cell activation. Consistent with previous reports, when PD-L1 expression and PD-1 checkpoint pathways were downregulated, T-cell activation was enhanced at 24 h after thermal ablation (Fig. 6B). Additionally, CD28 and EGF, which play key roles in the response to anti-PD-L1/PD-1 therapy [41, 42], exhibited decreased expression levels after thermal ablation. Metabolic pathways associated with pro-tumour phenotypes and poor prognosis during immune checkpoint blockade therapy, such as primary bile acid biosynthesis [43] and purine metabolism [22], showed the same tendency for decreased expression levels after ablation (Figure S3B, Cluster 4). Taken together, these data collectively indicate that thermal ablation in NSCLC functions in a synergistic manner with immune checkpoint blockade therapy, contributing to anti-tumour immunity.

Because chemokine receptors are expressed on various cells in the tumour microenvironment, chemokines affect diverse processes such as immune cell recruitment, angiogenesis, tumour cell survival, proliferation, and metastasis [44]. Chemokine systems contribute to cell adhesion and cell migration. In the present study, many chemokines (eg, CXCL1, 5, 9, 11, and 13 [45]; CCL3/4 [45]; and CX3CL1 [46]) with potential pro-tumour effects were decreased after thermal ablation; CXCL1, 5, 9, 11, and 13 interacted with the metabolite 5-Oxo-ETE (Fig. 5D). 5-Oxo-ETE is formed from the product of 5-lipoxygenase, 5-hydroxyeicosatetraenoic acid (5-HETE), by 5-hydroxyeicosanoid dehydrogenase; it is a chemoattractant for neutrophils, monocytes, and basophils, and it promotes tumour cell proliferation [47]. Notably, the metabolite 5-Oxo-ETE was decreased after

thermal ablation. The above evidence suggests that thermal ablation can downregulate proteins and metabolites with pro-tumourigenic chemotactic properties, thus exerting some anti-tumour effects at the molecular level. More rigorous and extensive validation of these molecules is needed in future studies.

In the present study, proteomic and metabolomic analyses showed that several plasma cytokines and metabolites involved in inflammatory responses were increased after ablation. A previous study revealed that IL-6 and IL-10 were elevated in plasma after thermal ablation; these trends were maintained for up to 5 weeks after the procedure [48], suggesting that the thermal ablation-induced inflammatory response persists for several weeks. 5'-Methylthioadenosine is a natural sulphur-containing nucleoside that affects multiple physiological responses, such as the inflammatory pathway, and regulates the activation of NF- κ B [49]. In the present study, the level of 5'-methylthioadenosine was substantially increased after ablation; it was correlated with the levels of pro-inflammatory factors IL-6 and placental growth factor. Multiple fatty acids (15-deoxy-delta-12,14-Pg₂, palmitic acid, and eicosapentaenoic acid) and steroid-related metabolites (corticosterone, cortisone, and cortisol) implicated in inflammatory responses also interacted with IL-6 (Fig. 6D). These findings suggest that pro-inflammatory proteins and metabolites interact after thermal ablation, leading to an enhanced systemic inflammatory response.

This study had some limitations. Based on a previous study [50], we assumed that the time point with the greatest change in plasma protein profile occurred 24 h after tumour ablation. Therefore, we collected plasma samples from patients before and 24 h after thermal ablation, with the goal of analysing the systemic effects of this procedure. In the future, more samples from various time points may be needed to fully explore the molecular dynamics after thermal ablation, including epithelial mesenchymal transition [51] and combination with other immunotherapy [52]. Patients in the present study will continue to attend follow-up; Additionally, we only collected plasma for proteomic and metabolomic analyses. We did not collect other biological samples (eg, lung tumour tissue or bronchoalveolar lavage fluid before and after thermal ablation) because necrosis after complete ablation hindered the acquisition of valid tumour tissue, and we did not routinely perform bronchoalveolar lavage after thermal ablation to reduce the risk of postoperative infection.

Currently, the main indications for thermal ablation include advanced tumours, multiple tumour foci,

and the presence of comorbidities that are not suitable for surgery. Considering the thermal ablation-induced alterations in the immune microenvironment of NSCLC observed in the present study, large-scale multicentre clinical trials and follow-up investigations of postoperative survival are needed to provide additional high-level evidence to support the recommendation of thermal ablation for the treatment of early-stage LC.

Conclusions

This study comprised a systematic proteomic and metabolomic investigation of plasma samples from NSCLC patients before and after thermal ablation, as well as HCs. Thermal ablation induces a systemic inflammatory response while decreasing the expression levels of pro-tumour protein pathways and metabolic pathways such as angiogenesis, immune checkpoint blockade, and pro-tumour chemotaxis. Our results suggest that thermal ablation-induced changes in the host plasma microenvironment contribute to anti-tumour immunity in NSCLC, offering new insights regarding tumour ablation combined with immunotherapy.

Abbreviations

NSCLC	Non-small cell lung cancer
CT	Computed tomography
ECG	Electrocardiogram
ENB	Electromagnetic navigation bronchoscope
EDTA	Ethylene diamine tetraacetic acid
LC	Lung cancer
LC-T	Lung cancer undergoing thermal ablation
HC	Healthy control
PEA	Proximity extension assay
NGS	Next-generation sequencing
NPX	Normalized protein expression
QC	Quality control
SD	Standard deviation
LC-MAS	Liquid chromatography-mass spectrometry
FC	Fold change
HMDB	The human metabolome database
DEP	Differentially expressed proteins
PLS-DA	Partial least squares-discriminant analysis
KEGG	The Kyoto Encyclopedia of genes and genome
DEM	Differently expressed metabolites
RDA	Redundancy analysis
5-Oxo-Etes	5-Oxo-6,8,11,14-eicosatetraenoic acid
BALF	Bronchoalveolar lavage fluid

Supplementary Information

The online version contains supplementary material available at <https://doi.org/10.1186/s12931-024-02917-9>.

Additional file 1.
Additional file 2.
Additional file 3.
Additional file 4.
Additional file 5.

Acknowledgements

We thank all individuals who participated in this study. We thank Hongjie Li, Huiwen Chu, and Wenjie Gu for assistance with thermal ablation. We thank Yan Li and her team (Fan-Xing Biological Technology Co.) for contributions to the bioinformatics analysis platform.

Author contributions

Jieqiong Li, Feng Wang, and Zhaohui Tong conceived and designed the study. Feng Wang performed the procedures and supervised the project. Xinglu Zhang, Shuai Shao, and Fengjiao Liu collected clinical specimens. Xinglu Zhang was responsible for the collection of clinical information and drafting the manuscript. Jieqiong Li performed bioinformatics analysis. Jieqiong Li, Nan Song, and Baolu Yang critically revised the manuscript. All authors contributed to the study and approved the final version of the manuscript.

Funding

This study was supported by Beijing Research Ward Demonstration Construction Project (No. BCRW202110).

Availability of data and materials

The raw data pertaining to the HPLC analyses and the raw data of the mass spectrometer have been uploaded as supplementary materials. Further datasets used and/or analysed during the current study are available from the corresponding author on reasonable request.

Declarations

Ethics approval and consent to participate

The study protocol was reviewed and approved by the Ethics Committee for Human Studies of Beijing Chaoyang Hospital, China (No. 2023-KE-432) in accordance with the Declaration of Helsinki. All patients in this study provided written informed consent before thermal ablation.

Consent for publication

Not applicable.

Competing interests

The authors declare no competing interests.

Author details

¹Department of Respiratory and Critical Care Medicine, Beijing Institute of Respiratory Medicine and Beijing Chao-Yang Hospital, Capital Medical University, No. 8 Gongti South Road, Beijing 100020, Chaoyang District, China. ²Medical Research Center, Beijing Institute of Respiratory Medicine and Beijing Chao-Yang Hospital, Capital Medical University, Beijing, China.

Received: 20 April 2024 Accepted: 15 July 2024

Published online: 14 August 2024

References

- Sung H, Ferlay J, Siegel RL, Laversanne M, Soerjomataram I, Jemal A, et al. Global cancer statistics 2020: globocan estimates of incidence and mortality worldwide for 36 cancers in 185 countries. *CA Cancer J Clin*. 2021;71(3):209–49.
- Oser MG, Niederst MJ, Sequist LV, Engelman JA. Transformation from non-small-cell lung cancer to small-cell lung cancer: molecular drivers and cells of origin. *Lancet Oncol*. 2015;16(4):e165–72.
- National Cancer Institute. Cancer Stat Facts: Lung and Bronchus Cancer. 2023. Available from URL: <https://seer.cancer.gov/statfacts/html/lungb.html>.
- Dupuy DE. Image-guided thermal ablation of lung malignancies. *Radiology*. 2011;260(3):633–55.
- Zerbini A, Pilli M, Penna A, Pelosi G, Schianchi C, Molinari A, et al. Radiofrequency thermal ablation of hepatocellular carcinoma liver nodules can activate and enhance tumor-specific T-cell responses. *Cancer Res*. 2006;66(2):1139–46.
- Thompson RH, Atwell T, Schmit G, Hohse CM, Kurup AN, Weisbrod A, et al. Comparison of partial nephrectomy and percutaneous ablation for cT1 renal masses. *Eur Urol*. 2015;67(2):252–9.
- Cao XJ, Wang SR, Che Y, Liu J, Cong ZB, He JF, et al. Efficacy and safety of thermal ablation for treatment of solitary T1N0M0 papillary thyroid carcinoma: a multicenter retrospective study. *Radiology*. 2021;300(1):209–16.
- Tsakok MT, Little MW, Hynes G, Millington RS, Boardman P, Gleeson FV, et al. Local control, safety, and survival following image-guided percutaneous microwave thermal ablation in primary lung malignancy. *Clin Radiol*. 2019;74(1):80.e19–80.e26.
- Rossi S, Dore R, Cascina A, Vespro V, Garbagnati F, Rosa L, et al. Percutaneous computed tomography-guided radiofrequency thermal ablation of small unresectable lung tumours. *Eur Respir J*. 2006;27(3):556–63.
- Ni Y, Peng J, Yang X, Wei Z, Zhai B, Chi J, et al. Multicentre study of microwave ablation for pulmonary oligorecurrence after radical resection of non-small-cell lung cancer. *Br J Cancer*. 2021;125(5):672–8.
- Yang W, Wang W, Liu B, Zhu B, Li J, Xu D, et al. Immunomodulation characteristics by thermal ablation therapy in cancer patients. *Asia Pac J Clin Oncol*. 2018;14(5):e490–7.
- Xu A, Zhang L, Yuan J, Babikr F, Freywald A, Chibbar R, et al. TLR9 agonist enhances radiofrequency ablation-induced CTL responses, leading to the potent inhibition of primary tumor growth and lung metastasis. *Cell Mol Immunol*. 2019;16(10):820–32.
- Wei Z, Yang X, Ye X, Huang G, Li W, Han X, et al. Camrelizumab combined with microwave ablation improves the objective response rate in advanced non-small cell lung cancer. *J Cancer Res Ther*. 2019;15(7):1629–34.
- Waitz R, Solomon SB, Petre EN, Trumble AE, Fassò M, Norton L, et al. Potent induction of tumor immunity by combining tumor cryoablation with anti-CTLA-4 therapy. *Cancer Res*. 2012;72(2):430–9.
- He YY, Yan Y, Chen JW, Liu S, Hua L, Jiang X, et al. Plasma metabolomics in the perioperative period of defect repair in patients with pulmonary arterial hypertension associated with congenital heart disease. *Acta Pharmacol Sin*. 2022;43(7):1710–20.
- Wu Y, Cao F, Zhou D, Chen S, Qi H, Huang T, et al. Cryoablation reshapes the immune microenvironment in the distal tumor and enhances the anti-tumor immunity. *Front Immunol*. 2022;13: 930461.
- Dong Y, Lu J, Wang T, Huang Z, Chen X, Ren Z, et al. Multi-omics analysis reveals disturbance of nanosecond pulsed electric field in the serum metabolic spectrum and gut microbiota. *Front Microbiol*. 2021;12: 649091.
- Wu SY, Fu T, Jiang YZ, Shao ZM. Natural killer cells in cancer biology and therapy. *Mol Cancer*. 2020;19(1):120.
- Zhang T, Nie Y, Gu J, Cai K, Chen X, Li H, et al. Identification of mitochondrial-related prognostic biomarkers associated with primary bile acid biosynthesis and tumor microenvironment of hepatocellular carcinoma. *Front Oncol*. 2021;11: 587479.
- Mossmann D, Müller C, Park S, Ryback B, Colombi M, Ritter N, et al. Arginine reprograms metabolism in liver cancer via RBM39. *Cell*. 2023;186(23):5068–83.e23.
- Elia I, Broekaert D, Christen S, Boon R, Radaelli E, Orth MF, et al. Proline metabolism supports metastasis formation and could be inhibited to selectively target metastasizing cancer cells. *Nat Commun*. 2017;8:15267.
- Li S, Yu J, Huber A, Kryczek I, Wang Z, Jiang L, et al. Metabolism drives macrophage heterogeneity in the tumor microenvironment. *Cell Rep*. 2022;39(1): 110609.
- Heijink DM, Fehrmann RS, de Vries EG, Koornstra JJ, Oosterhuis D, van der Zee AG, et al. A bioinformatical and functional approach to identify novel strategies for chemoprevention of colorectal cancer. *Oncogene*. 2011;30(17):2026–36.
- Nava Lauson CB, Tiberti S, Corsetto PA, Conte F, Tyagi P, Machwirth M, et al. Linoleic acid potentiates CD8(+) T cell metabolic fitness and antitumor immunity. *Cell Metab*. 2023;35(4):633–50.e9.
- Guo K, Chen D, Ren S, Younis MR, Teng Z, Zhang L, et al. Reversing immune suppression and potentiating photothermal immunotherapy via bispecific immune checkpoint inhibitor loaded hollow polydopamine nanospheres. *ACS Appl Mater Interfaces*. 2023. <https://doi.org/10.1021/acami.2c19790>.

26. Gao Q, Zhang Y. CXCL11 signaling in the Tumor microenvironment. *Adv Exp Med Biol.* 2021;1302:41–50.
27. Tokunaga R, Zhang W, Naseem M, Puccini A, Berger MD, Soni S, et al. CXCL9, CXCL10, CXCL11/CXCR3 axis for immune activation—a target for novel cancer therapy. *Cancer Treat Rev.* 2018;63:40–7.
28. Sun L, Zhang H, Gao P. Metabolic reprogramming and epigenetic modifications on the path to cancer. *Protein Cell.* 2022;13(12):877–919.
29. Grant GE, Rokach J, Powell WS. 5-Oxo-EETE and the OXE receptor. *Prostaglandins Other Lipid Mediat.* 2009;89(3–4):98–104.
30. Taniguchi K, Karin M. IL-6 and related cytokines as the critical lymphins between inflammation and cancer. *Semin Immunol.* 2014;26(1):54–74.
31. Venturini M, Cariati M, Marra P, Masala S, Pereira PL, Carrafiello G. CIRSE standards of practice on thermal ablation of primary and secondary lung tumours. *Cardiovasc Intervent Radiol.* 2020;43(5):667–83.
32. Genshaft SJ, Suh RD, Abtin F, Baerlocher MO, Chang AJ, Dariushnia SR, et al. Society of interventional radiology multidisciplinary position statement on percutaneous ablation of non-small cell lung cancer and metastatic disease to the lungs: endorsed by the Canadian association for interventional radiology, the cardiovascular and interventional radiological society of Europe, and the society of interventional oncology. *J Vasc Interv Radiol.* 2021. <https://doi.org/10.1016/j.jvir.2021.04.024>.
33. Eberhardt WE, De Ruysscher D, Weder W, Le Péchoux C, De Leyn P, Hoffmann H, et al. 2nd ESMO consensus conference in lung cancer: locally advanced stage III non-small-cell lung cancer. *Ann Oncol.* 2015;26(8):1573–88.
34. Murphy MC, Wrobel MM, Fisher DA, Cahalane AM, Fintelmann FJ. Update on image-guided thermal lung ablation: society guidelines, therapeutic alternatives, and postablation imaging findings. *AJR Am J Roentgenol.* 2022;219(3):471–85.
35. Daly C, Eichten A, Castanaro C, Pasnikowski E, Adler A, Lalani AS, et al. Angiopoietin-2 functions as a Tie2 agonist in tumor models, where it limits the effects of VEGF inhibition. *Cancer Res.* 2013;73(1):108–18.
36. Nissen LJ, Cao R, Hedlund EM, Wang Z, Zhao X, Wetterskog D, et al. Angiogenic factors FGF2 and PDGF-BB synergistically promote murine tumor neovascularization and metastasis. *J Clin Invest.* 2007;117(10):2766–77.
37. Lurje G, Leers JM, Pohl A, Oezcelik A, Zhang W, Ayazi S, et al. Genetic variations in angiogenesis pathway genes predict tumor recurrence in localized adenocarcinoma of the esophagus. *Ann Surg.* 2010;251(5):857–64.
38. Tran AN, Boyd NH, Walker K, Hjelmeland AB. NOS expression and no function in glioma and implications for patient therapies. *Antioxid Redox Signal.* 2017;26(17):986–99.
39. Lyu N, Kong Y, Li X, Mu L, Deng H, Chen H, et al. Ablation reboots the response in advanced hepatocellular carcinoma with stable or atypical response during PD-1 therapy: a proof-of-concept study. *Front Oncol.* 2020;10: 580241.
40. Xiao W, Huang H, Zheng P, Liu Y, Chen Y, Chen J, et al. The CXCL10/CXCR3 pathway contributes to the synergy of thermal ablation and PD-1 blockade therapy against Tumors. *Cancers.* 2023. <https://doi.org/10.3390/cancers15051427>.
41. Hui E, Cheung J, Zhu J, Su X, Taylor MJ, Wallweber HA, et al. T cell costimulatory receptor CD28 is a primary target for PD-1-mediated inhibition. *Science.* 2017;355(6332):1428–33.
42. Chen M, Sharma A, Lin Y, Wu Y, He Q, Gu Y, et al. Insulin and epithelial growth factor (EGF) promote programmed death ligand 1 (PD-L1) production and transport in colon cancer stem cells. *BMC Cancer.* 2019;19(1):153.
43. Sun R, Zhang Z, Bao R, Guo X, Gu Y, Yang W, et al. Loss of SIRT5 promotes bile acid-induced immunosuppressive microenvironment and hepatocarcinogenesis. *J Hepatol.* 2022;77(2):453–66.
44. Borsig L, Wolf MJ, Roblek M, Lorentzen A, Heikenwalder M. Inflammatory chemokines and metastasis—tracing the accessory. *Oncogene.* 2014;33(25):3217–24.
45. Ozga AJ, Chow MT, Luster AD. Chemokines and the immune response to cancer. *Immunity.* 2021;54(5):859–74.
46. Wang K, Jiang L, Hu A, Sun C, Zhou L, Huang Y, et al. Vertebral-specific activation of the CX3CL1/ICAM-1 signaling network mediates non-small-cell lung cancer spinal metastasis by engaging tumor cell-vertebral bone marrow endothelial cell interactions. *Theranostics.* 2021;11(10):4770–89.
47. Powell WS, Rokach J. The eosinophil chemoattractant 5-oxo-EETE and the OXE receptor. *Prog Lipid Res.* 2013;52(4):651–65.
48. Erinjeri JP, Thomas CT, Samoilia A, Fleisher M, Gonen M, Sofocleous CT, et al. Image-guided thermal ablation of tumors increases the plasma level of interleukin-6 and interleukin-10. *J Vasc Interv Radiol.* 2013;24(8):1105–12.
49. Rattajak P, Aroonkesorn A, Smythe C, Witisuwannakul R, Pitakpornpreecha T. 5'-Methylthioadenosine strongly suppresses RANKL-induced osteoclast differentiation and function via inhibition of RANK-NFATc1 signalling pathways. *Heliyon.* 2023;9(11): e22365.
50. Wah TM, Zhong J, Wilson M, Vasudev NS, Banks RE. An exploratory analysis of changes in circulating plasma protein profiles following image-guided ablation of renal tumours provides evidence for effects on multiple biological processes. *Cancers.* 2021. <https://doi.org/10.3390/cancers13236037>.
51. Xue W, Yang L, Chen C, Ashrafzadeh M, Tian Y, Sun R. Wnt/ β -catenin-driven EMT regulation in human cancers. *Cell Mol Life Sci.* 2024;81(1):79.
52. Lu Q, Kou D, Lou S, Ashrafzadeh M, Aref AR, Canadas I, et al. Nanoparticles in tumor microenvironment remodeling and cancer immunotherapy. *J Hematol Oncol.* 2024;17(1):16.

Publisher's Note

Springer Nature remains neutral with regard to jurisdictional claims in published maps and institutional affiliations.